Phys Chem Minerals (2018) 45:85–92
https://doi.org/10.1007/s00269-017-0904-3

REVIEW ARTICLE

Migration of impurity level reflected in the electrical conductivity variation for natural pyrite at high temperature and high pressure

Kaixiang Liu[1,2] · Lidong Dai[1] · Heping Li[1] · Haiying Hu[1] · Lei Wu[1] · Yukai Zhuang[1,2] · Chang Pu[1,2] · Linfei Yang[1,2]

Received: 21 February 2017 / Accepted: 5 June 2017 / Published online: 13 June 2017

Abstract This report presents the variations of the electrical conductivity and the migration of natural pyrite impurity levels at temperatures range from 298 to 573 K and pressures range from 1 atm. to 20.9 GPa. The electrical conductivity increases with temperature at a fixed pressure, displaying the semiconductor behavior of the sample. In spite of the positive correlations of electrical conductivity and pressure, there exists an acceleration in the rate of conductivity increase after ~13 GPa. No indication of a chemical reaction or structural phase transition of pyrite was detected by Raman spectroscopy. The main trace elements that affect the electrical properties of pyrite are determined by inductively coupled plasma with mass spectrometry (ICPMS). The transport activation energy of natural pyrite is ~0.045 eV at ambient pressure, which corresponds to the activation of the Co_{Fe} donor level (~1/2 E_D), and decreases with increasing pressure.

Keywords Pyrite · Electrical conductivity · Impurity level · High temperature and high pressure

Introduction

Iron disulfide (FeS_2) in the form of pyrite, which belongs to transition metal sulfides and is the most abundant type of sulfide in the Earth's crust. FeS_2 occurs in various geological environments (sedimentary, metamorphic, magmatic and hydrothermal deposits). The Fe-S system may have played an important role in the formation and evolution of the earth's core and other terrestrial planets, such as Venus and Mars (Ahrens and Jeanloz 1987). Therefore, it is crucial to study the physical and chemical properties of pyrites under high temperature and high pressure. Previous studies have verified that, under ambient pressure conditions, pyrrhotite decomposition from pyrite is completed at approximately 973 K (Li and Zhang 2005). As an effective means of changing the thermodynamic properties of the material, the effect of pressure on the properties of pyrite has attracted considerable interest (Clendenen and Drickamer 1966; Sawaoka et al. 1974; Chattopadhyay and Schnering 1985; Jephcoat and Olson 1987; Kleppe and Jephcoat 2004). Previous studies on pyrite mainly focused on its structural phase transformations at high pressure and have confirmed that the structure of pyrite is stable, with no new phases appearing until ~180 GPa (Clendenen and Drickamer 1966; Sawaoka et al. 1974; Chattopadhyay and Schnering 1985; Jephcoat and Olson 1987; Merkel et al. 2002; Kleppe and Jephcoat 2004). Meanwhile, as a new photovoltaic material for solar cells, the valence band structure and electrical properties of pyrite have also aroused widespread attention (Pridmore and Shuey 1976; Cervantes et al. 2002). Natural pyrite is an indirect band gap semiconductor with an energy gap E_g of approximately 0.80–0.93 eV (Pridmore and Shuey 1976; Ennaoui and Tributsch 1986; Ennaoui et al. 1993; Schieck et al. 1990). As, Ni, Co, Cu and other trace elements have large influences on the electrical properties of pyrite, which determine the semiconductor type of pyrite (Abraitis et al. 2004; Savage et al. 2008). The substitution of As with S in pyrite would result in p-type semiconductor behavior and add a hole in the Fe

✉ Lidong Dai
dailidong@vip.gyig.ac.cn

[1] Key Laboratory of High-Temperature and High-Pressure Study of the Earth's Interior, Institute of Geochemistry, Chinese Academy of Sciences, Guiyang 550081, Guizhou, China

[2] University of Chinese Academy of Sciences, Beijing 100049, China

d-like valence band (Lehner et al. 2012). Ni substitutes for Fe and generates a deep level defect band (Yu et al. 1992). Substituting Co or Cu for Fe would result in an n-type semiconductor (Savage et al. 2008). However, regardless of the doping type of impurity ions, the conductivity of natural pyrite is dominated by Co (Savage et al. 2008). Although the electrical properties of natural pyrite under ambient pressure have been studied intensively, its electrical properties are still scarce at high temperature and high pressure. Cervantes et al. (2002) have determined the indirect energy gap and resistivities of pyrite at high pressure, which indicates that the band gap of the pyrite decreases linearly with pressure at a rate of $-1.13(9) \times 10^{-2}$ eV/GPa, and the resistivity of the pyrite decreases with pressure, while a slowdown in deceleration occurs after ~14 GPa. Based on this, there are several interesting and unresolved questions to do with natural pyrite: (1) does temperature have an effect on the structure and electrical properties of pyrite under high pressure? (2) What is the effect of the impurity levels on the electrical properties of pyrite under high pressure? In this study, we measured the electrical conductivities (1 atm.–20.9 GPa, 298–573 K) and Raman spectra (1 atm.–15.9 GPa, 298–573 K) of pyrite at high temperature and high pressure. The variations of the conductivities of pyrite under high temperature and high pressure and the role of impurity levels are discussed in detail.

Experimental procedure

Sample descriptions

Natural pyrite is the cubic crystal symmetry (space group Pa3). The Fe^{2+} cation occupies a site on the face-centered-cubic sublattice, and the S_2^{-2} dimers are centered at the midpoints of the cube edges and body centers.

The natural pyrite used in the experiment was collected from Dajiangping Diggings in Yunfu city, Guangdong province. The main trace elements that affect the electrical properties of this pyrite were determined by ICPMS in the State Key Laboratory of Ore Deposit Geochemistry, Institute of Geochemistry, Chinese Academy of Sciences.

High-pressure Raman spectra measurements

The high-temperature and high-pressure Raman studies were carried out using a 300 μm diamond anvil cell (DAC) with an external electric resistance heating furnace. A ruby crystal was chosen for pressure calibration through the wavenumber shift of the fluorescence bands of the Cr^{3+} ions. Two pieces of prepressed NaCl chips were adopted as the pressure transmitting medium. The Raman spectra were collected using a Raman spectrometer (Invia, Renishaw) equipped with a confocal microscope (TCS SP8, Leica) and a CCD camera (Olympus). In the simultaneously high temperature and high pressure experiments, the sample cell load was increased to a certain pressure, the diamond anvils were held fixed, and the temperature was gradually raised to 573 K by intervals of 50 K. The excitation laser powers were typically 20 mW for the Raman spectra and 0.5–40 μW for fluorescence. Spectra were taken for the backscattering geometry using an argon ion laser (spectra physics: 514.5 nm, power <1 mW) in the range of 100–500 cm^{-1} with a spectral resolution of 1.0 cm^{-1}. Each acquisition was collected for 30 s, and at each measurement, the sample was held at a correspondent pressure for 900 s to achieve the stable equilibrium. The Raman spectra were fitted by the PeakFit software.

High-pressure electrical conductivity measurements

High pressure experiments were conducted in a DAC with a 300 μm diameter anvil culet. The sample was crushed into a powder (~20 μm). A T-301 stainless steel gasket was pre-indented to a thickness of ~60 μm, and a 180 μm hole was drilled with a laser. A mixture of boron nitride powder and epoxy was then compressed into the hole, and another 100 μm hole was drilled as an insulating sample chamber.

Figure 1 shows a cross-sectional assembly of the designed DAC used in this study. AC impedance

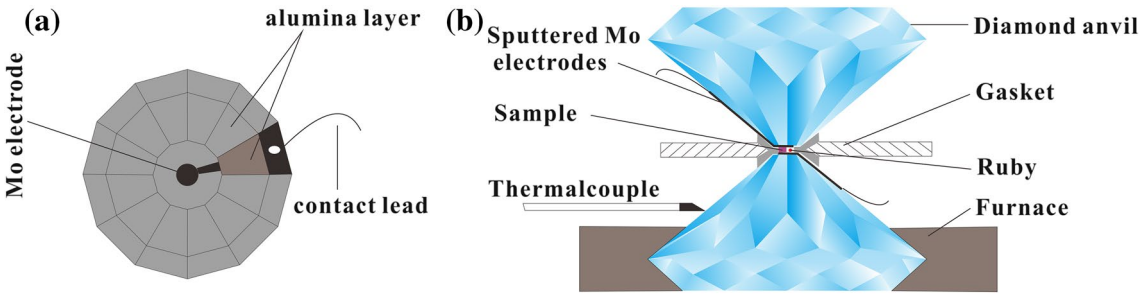

Fig. 1 Experimental assembly for electrical conductivity measurement. **a** Configuration of plate electrodes integrated on two diamond anvils. **b** Cross section of the DAC used for high-temperature and high-pressure impedance spectroscopy measurement

spectroscopy was performed with a system consisting of an impedance spectrometer (1260, Solartron) in combination with a dielectric interface (1296, Solartron) at frequencies of 10^{-1} to 10^{7} Hz. The plate electrode was integrated into both diamond anvils (Li et al. 2006). A k-type thermocouple with an estimated accuracy of 5 K was attached to the side of the diamond anvil used for the temperature measurements. Circulating water was used to maintain the thermal stability of the DAC at high temperature. The specific measurement procedure is described elsewhere (Dai et al. 2016a, b; Wu et al. 2016, 2017).

Results and discussion

Figure 2a shows the Raman spectra of pyrite as a function of pressure during both the compression and decompression processes. Three peaks could be resolved in the spectra: the 343, 379 and 430 cm^{-1} peaks represent the E_g, A_g and $T_{g(3)}$ modes of pyrite, respectively. All the Raman modes shift continuously towards higher frequencies with increasing pressure, which agrees well with previous studies (Kleppe and Jephcoat 2004). It can be seen from Fig. 2a that the decompressed Raman spectra of pyrite is recovered to its original state, which indicates a reversible process. The $\partial\omega/\partial P$ slopes for the E_g, A_g and $T_{g(3)}$ modes of pyrite at room temperature during the processes of compression and decompression are shown in Table 1. Figure 2b shows the representative Raman spectra of pyrite over different temperatures at ~8.9 GPa. The modes shift to lower frequencies with temperature increases at a constant pressure. The $T_{g(3)}$ mode of pyrite was weak and not continuously observed at high temperature and high pressure, and; however, only the E_g and A_g modes remained sharp and clear. The temperature dependences of the Raman modes of pyrite are shown in Fig. 2c and the $\partial\omega/\partial T$ slopes for the E_g and A_g modes of pyrite at 8.9 GPa are displayed in Table 1. The positive correlations of all the vibrational modes to pressure indicate

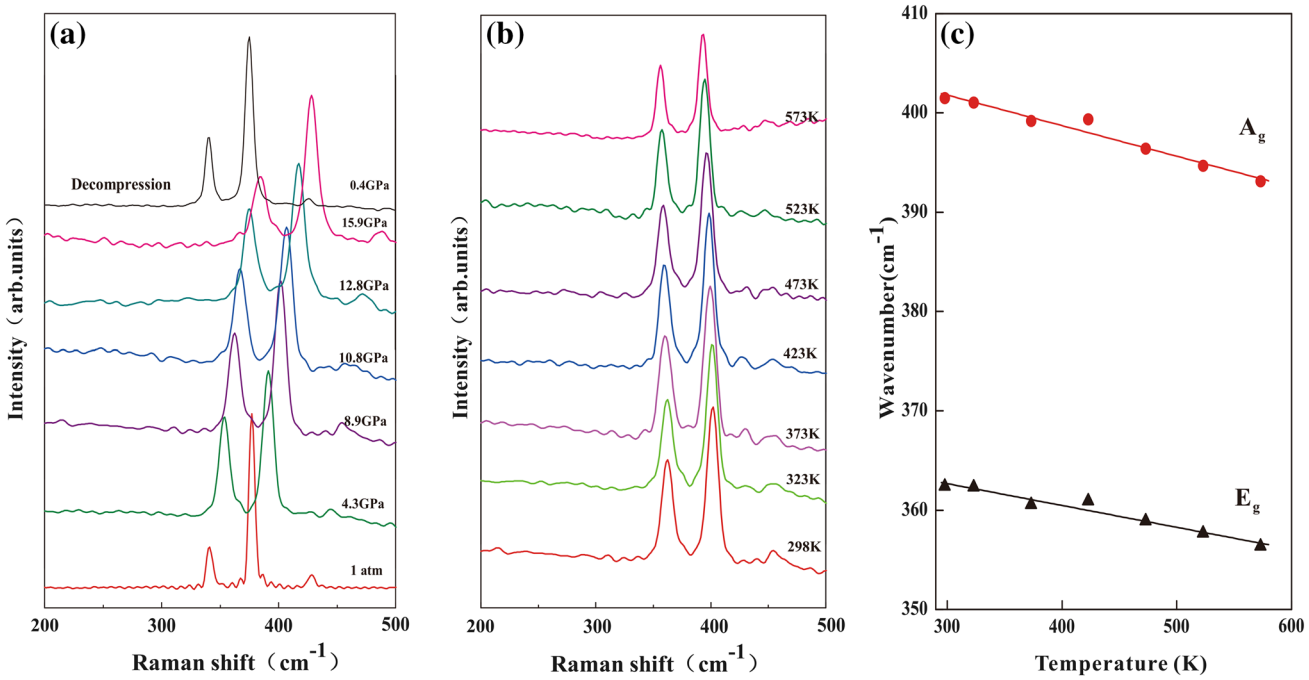

Fig. 2 **a** Raman spectra at different pressure at 298 K in the process of compression and decompression. **b** Raman spectra at different temperatures with pressure of ~8.9 GPa. **c** Temperature dependence of the Raman modes of pyrite at 8.9 GPa. Errors in both frequency and pressure are within the size of symbol

Table 1 Temperature and pressure dependence of Raman shift

Raman mode	$\partial\omega/\partial P$ (cm^{-1}/GPa) of compression	$\partial\omega/\partial P$ (cm^{-1}/GPa) of decompression	$\partial\omega/\partial T$ (cm^{-1}/GPa) at 8.9 GPa
Eg	2.65 (0.20)	2.72 (0.12)	−0.022 (0.002)
Ag	3.13 (0.22)	3.27 (0.15)	−0.031 (0.002)
$Tg_{(3)}$	3.67 (0.31)	3.73 (0.25)	–

pressure-induced contractions for the Fe–S and S–S bonds of pyrite under compression, while the negative correlation between the vibration modes and temperature shows temperature-induced expansions of the Fe–S and S–S bonds of pyrite (Utyuzh 2014).

Previous studies have shown that pyrite is stable under a wide pressure range (Clendenen and Drickamer 1966). Our results show that the E_g, A_g and $T_{g(3)}$ modes of pyrite continuously shift to higher frequencies with increasing pressure, or conversely, to lower frequencies with increasing temperature at a constant pressure. No indication of chemical reaction or structure phase transition of pyrite was detected. The results further demonstrate that pyrite is stable under our experimental conditions.

The impedance spectra from different temperature and pressure conditions are displayed in Fig. 3. In the pressure

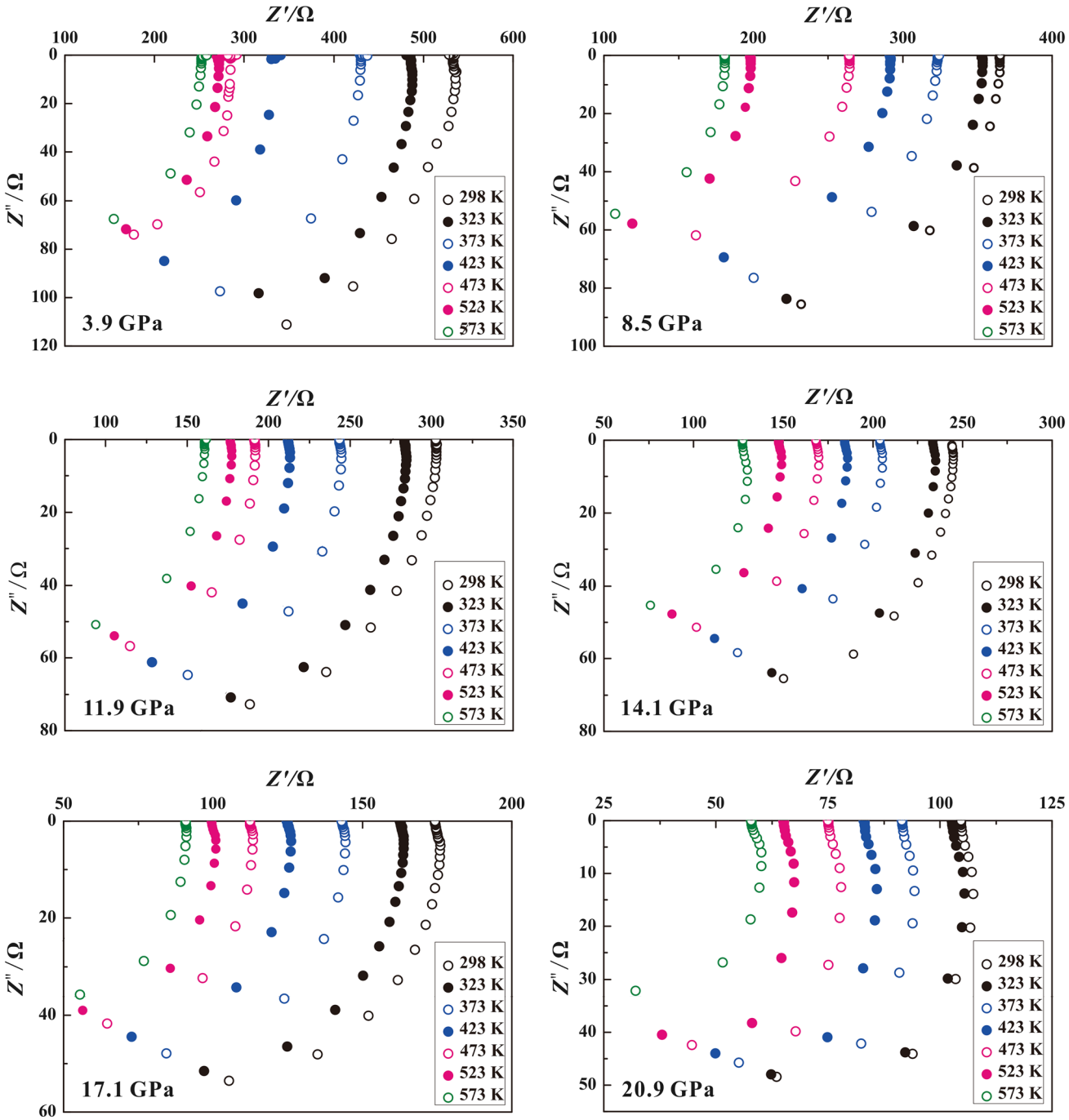

Fig. 3 Selected impedance spectra (Nyquist plots) in the complex plane of pyrite at different pressures and temperatures

range of this study, the impedance spectra appeared only in the fourth quadrant, which represents the electron response of the sample (Pommier et al. 2010), and did not show the semicircular arc in the high frequency region (Dai et al. 2013, 2016a, b, c). This phenomenon indicates that the electronic crystal structure of pyrite remains stable. The equivalent circuit of the impedance spectra is a simple resistor. The value of resistance is obtained for $Z'' = 0$ and the influence of the wire resistance has been fully considered (Pommier et al. 2010).

The electrical conductivity of the parallel plate electrode can be obtained as follows:

$$\sigma = \frac{1}{R}\left(\frac{l}{A}\right), \tag{1}$$

where A and l denote the electrode area and the distance between the two electrodes, respectively.

Figure 4a shows the relationship between the total electrical conductivity and reciprocal temperature for pyrite from 323 to 573 K under different pressures. The conductivity of pyrite under different pressures is in accord with the Arrhenius relationship. The conductivity shows a positive relationship with temperature over the entire pressure range, indicating the semiconductor behavior of the sample, but no pressure-induced semiconductor to metal transition (Cervantes et al. 2002). Based on the temperature dependence of the conductivity, the transport activation energy of pyrite at a given pressure can be obtained from:

$$\sigma = \sigma_0 \exp(-E_t/k_b T), \tag{2}$$

where σ_0 is the pre-exponential factor (Sm^{-1}), E_t is the transport activation energy (eV), k_b is the Boltzmann constant and T is the absolute temperature (K). The value of E_t can be obtained by linearly fitting the plot of the logarithmic conductivity vs. 1000/T. Figure 4b shows transport activation energy decreases with pressure for pyrite, which indicates that, as the distance between the atoms becomes closer, the overlap of the electron orbital wave function increases, the energy band widens and the energy gap narrows. E_t is determined by the defect energy levels in the energy gap (Chen et al. 1993). It is well known that natural pyrite is an indirect band gap semiconductor. According to the principles of semiconductor physics, the electrical properties of pyrite depend on the defects in its crystal structure caused by the substitution of impurities for Fe or S. These impurities will introduce impurity levels into the forbidden band, and the impurity level could release electrons to the conduction band or add holes to the valence band, some of which radically alter electrical properties (Sze and Kwok 2007). Previous studies have shown the electron transportation characteristics of natural pyrite and synthetic pyrite are dominated by impurity defects such as As, Ni, Co and Cu (Abraitis et al. 2004; Savage et al. 2008). It does not imply that other metallic element impurities cannot change electrical properties, but some detailed measurements of their effects are not yet conducted. In arsenian $FeAs_xS_{2-x}$ and arsenopyrite $Fe(S,As)_2$, As substitutes for S and is almost always p-type as a result (Lehner et al. 2006), and the primary function of As is to add a hole to the Fe d-like valence band. Ni substitutes for Fe (Ni_{Fe}) and generates a deep level defect band that must be incompletely ionized at room temperature (Yu et al. 1992) and, therefore, Ni_{Fe} has no obvious effect on the carrier concentration (Savage et al. 2008). Recently, Hall measurements vs. temperature performed

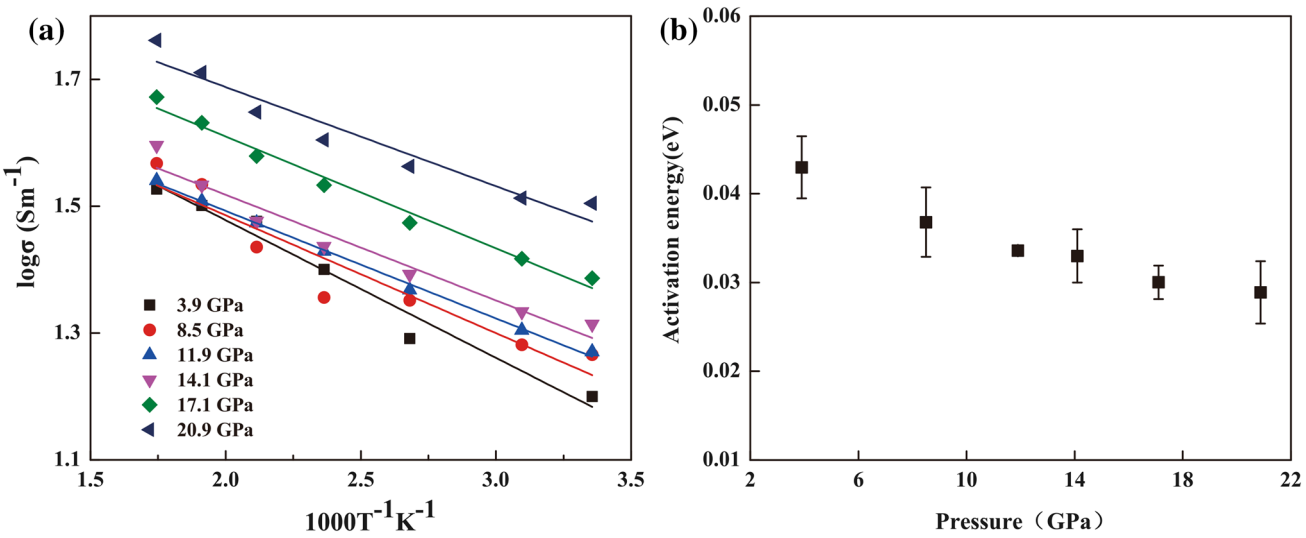

Fig. 4 **a** Temperature-dependent conductivity under different pressure in the Arrhenius relation for pyrite. **b** Transport activation energies as a function of pressure of pyrite. Errors in conductivities and temperatures are smaller than the size of the *symbols*

by Lehner et al. (2012) confirmed that Ni_{Fe} results in deep-levels at 0.37 and 0.42 eV below the conduction band (CB) edge. Co and Cu substitution with Fe (Co_{Fe} and Cu_{Fe}) are both partially ionized at room temperature, resulting in n-type behaviors. Regardless of which type of impurity doping occurs, the conductivity of natural pyrite is dominated by Co (Savage et al. 2008). Lehner et al. (2012) have determined that Co introduces a partially filled Co_{Fe} donor level at 0.09 eV (E_D) below the conduction band minimum (CBM). From the relationship between the transport activation energy and pressure, as shown in Fig. 4b, we calculated that the transport activation energy of pyrite is ~0.045 eV at atmospheric pressure, corresponding with the activation of the Co_{Fe} donor level (~1/2 E_D) (Lehner et al. 2012).

Figure 5a shows the pressure-dependent logarithm of conductivity at room temperature. The conductivity of this experimental sample is smaller than that of Cervantes et al. (2002) by ~2 orders of magnitude in the entire pressure region and is consistent with experimental results of Savage et al. (2008) at ambient pressure. Figure 5b shows the pressure-dependent conductivity at different temperatures. Notice that the temperature changes will bring about certain pressure oscillations at each pressure point, so we modified the pressure value at each temperature. As shown in Fig. 5b, the conductivity of pyrite at 298 K increases gradually from ambient pressure to ~13 GPa at the rate of ~0.36 S m^{-1} GPa^{-1}, followed by a higher rate (~1.68 S m^{-1} GPa^{-1}) of increase above this pressure. The higher rate of pressure independent conductivity can be attributed to the chemical defects of pyrite rather than the volumetric compression (Cervantes et al. 2002). Previous studies have shown that the electronic transportation characteristics of natural pyrite and synthetic pyrite are dominated by impurity defects (Abraitis et al. 2004; Savage et al. 2008). The initial increase in conductivity with pressure, before ~13 GPa, is attributed to the increasing overlap of the electron orbital wave function and the narrowing energy gap of the Co impurity (Cervantes et al. 2002). After ~13 GPa, the Fermi level crosses the Co donor level, ionizing additional electrons into the conduction band, resulting in an increase of conductivity.

Previous studies have shown that most natural pyrite is an n-type semiconductor (Ferrer et al. 1990; Delasheras et al. 1994; Karguppikar and Vedeshwar 1988). Depending on the type of impurities, the donor energy level is 5–200 meV below the conduction band (Ferrer et al. 1990). In the case of our sample, the transport activation energy of pyrite at ambient pressure is ~0.045 eV, which agrees with the activation of the donors (~1/2 E_D), characteristic of uncompensated material (Lehner et al. 2012). The measured impurity concentrations of FeS_2 in this study are shown in Table 2. Referencing previous studies (Savage et al. 2008; Lehner et al. 2012) and the results of this study, we consider that the donor level related to the conductivity of this sample to be Co. While Co is not present in the sample of Cervantes et al. (2002), its conductivity was higher than that of our sample. This may be due to other high content impurity determining the conductivity of the sample of Cervantes et al. (2002) and the small content (40.6 ppm) of Co in ours. The unknown impurity level may ionize at

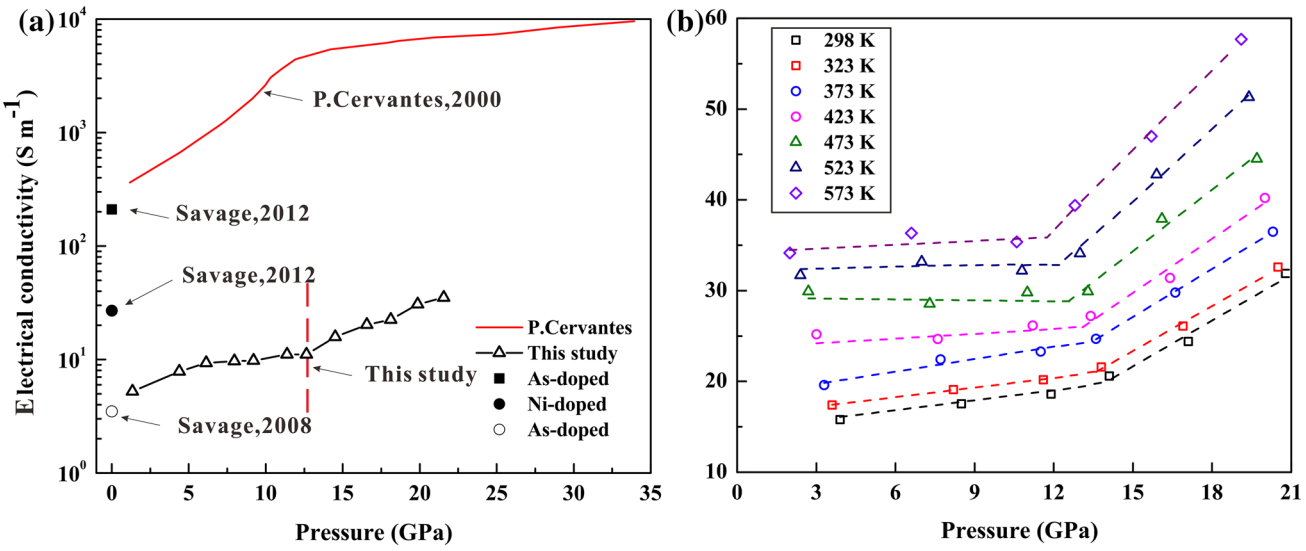

Fig. 5 **a** Pressure-dependent logarithm of conductivity at room temperature of present work (*open triangle*) and previous work (*red line*, Cervantes et al. 2002; *black square*, 340 ppm As-doped, Lehner et al. 2012; *black circle*, 4100 ppm Ni-doped, Lehner et al. 2012; *open circle*, As-9 with 658 ppm As, 83 ppm Co and 200 ppm Ni, Savage et al. 2008). **b** Pressure-dependent conductivity at different temperatures. Errors in conductivities and pressures are smaller than the size of the *symbols*

Table 2 Main trace elements of pyrite determined by ICPMS

Element constituent	Concentration (ppm)
As	480.3
Co	46.1
Cu	40.7
Sn	14.6
Ni	13.5
Sb	5.33
Sc	4.82
V	4.18
W	4.12
La	3.69
U	3.37
Pb	2.72
Nd	2.64
Sr	2.57
Ag	1.84
Cd	1.76
Bi	1.69
Dy	1.63
Sm	1.33
Er	1.29
Pr	1.25
Hf	1.25
Mo	1.22
Th	1.22
Yb	1.18
Y	1.14
Gd	1.12
Ce	1.03
Ge	0.80
Ta	0.71
Ba	0.69
Nb	0.56
Rb	0.47
Zr	0.39
Ho	0.38
Cs	0.32
Ga	0.31
Zn	0.29
Li	0.28
Tb	0.24
Cr	0.22
Tm	0.18
Lu	0.18
Be	0.17
In	0.14
Eu	0.09
Tl	0.09
Rh	–

lower pressure, which will cause the discrepancy of conductivity slopes, as shown in Fig. 5a.

The pressure dependence of the conductivity of pyrite at higher temperature is similar to that at 298 K except for the shift in where the slope changes, which occur at lower pressure. Many models and experiments can be used to reasonably explain the variations of the shift point. The gap of pyrite decreases in energy with increasing temperature, as it is a characteristic of semiconductors (Ravindra and Srivastava 1981). The crossing of Fermi level to Co donor level occurs at lower pressure and higher temperature, which will result in additional electrons entering the conduction band. This is the fundamental cause of the shift point varying with temperature.

Conclusions

In conclusion, the electrical conductivities of natural pyrite increase with pressure, and the increasing trend is more significant after ~13 GPa. This trend is highly correlated to the energy level of the Co impurity in pyrite, which releases more electrons to the conduction band under increasing pressure. This trend is not reflected in Raman spectra and is thus considered to be an electronic structural transition, and temperature can advance this transition. In addition, the conductivity of pyrite shows a positive relationship with temperature over the entire pressure range. Our calculated Co-related transport activation energy is ~0.045 eV at ambient pressure and decreases as a function of pressure. When E_t is reduced to zero, the Co impurity level intersects the conduction band, and conductivity does not change with temperature due to the saturation of the carrier density.

Acknowledgements We thank the editor of Larissa Dobrzhinetskaya and two anonymous reviewers for their very valuable and enlightened comments and suggestions in the reviewing process, which greatly improve the manuscript. We are also grateful to Springer Nature Author Services (SNAS) for their professional helps in English improvements of the manuscript. This research was financially supported by the Strategic Priority Research Program (B) of the Chinese Academy of Sciences (XDB 18010401), Key Research Program of Frontier Science of CAS (QYZDB-SSW-DQC009), "135" Program of the Institute of Geochemistry of CAS, Hundred Talents Program of CAS, NSF of China (41474078, 41304068 and 41174079) and the special fund of the West Light Foundation of CAS.

References

Abraitis P, Pattrick R, Vaughan D (2004) Variations in the compositional, textural and electrical properties of natural pyrite: a review. Int J Miner Process 74:41–59

Ahrens T, Jeanloz R (1987) Pyrite: shock compression, isentropic release, and composition of the Earth's core. J Geophys Res Solid Earth 92:10363–10375

Cervantes P, Slanic Z, Bridges F, Knittle E, Williams Q (2002) The band gap and electrical resistivity of FeS_2-pyrite at high pressures. J Phys Chem Solids 63:1927–1933

Chattopadhyay T, Schnering H (1985) High pressure X-ray diffraction study on p-FeS_2, m-FeS_2 and MnS_2 to 340 kbar: a possible high spin-low spin transition in MnS_2. J Phys Chem Solids 46:113–116

Chen A, Yu P, Taylor R (1993) Closure of the charge-transfer energy gap and metallization of NiI_2 under pressure. Phys Rev Lett 71:4011–4014

Clendenen R, Drickamer H (1966) Lattice parameters of nine oxides and sulfides as a function of pressure. J Chem Phys 44:4223–4228

Dai L, Li H, Hu H, Jiang J, Hui K, Shan S (2013) Electrical conductivity of $Alm_{82}Py_{15}Grs_3$ almandine-rich garnet determined by impedance spectroscopy at high temperatures and high pressures. Tectonophysics 608:1086–1093

Dai L, Hu H, Li H, Wu L, Hui K, Jiang J, Sun W (2016a) Influence of temperature, pressure, and oxygen fugacity on the electrical conductivity of dry eclogite, and geophysical implications. Geochem Geophys Geosyst 17:2394–2407

Dai L, Wu L, Li H, Hu H, Zhuang Y, Liu K (2016b) Evidence of the pressure-induced conductivity switching of yttrium-doped $SrTiO_3$. J Phys Condens Matter 28:475501. doi:10.1088/0953-8984/28/47/475501

Dai L, Wu L, Li H, Hu H, Zhuang Y, Liu K (2016c) Pressure-induced phase-transition and improvement of the micro dielectric properties in yttrium-doped $SrZrO_3$. EPL (Europhysics Letters) 114:56003. doi:10.1209/0295-5075/114/56003

Delasheras C, Ferrer I, Sanchez C (1994) Temperature dependence of the optical absorption edge of pyrite FeS_2 thin films. J Phys Condens Matter 6:10177–10183

Ennaoui A, Tributsch H (1986) Energetic characterization of the photoactive FeS_2 (pyrite) interface. Solar Energy Mater 14:461–474

Ennaoui A, Fiechter S, Pettenkofer C, Alonso V, Büker K (1993) Iron disulfide for solar energy conversion. Sol Energy Mater Sol Cells 29:289–370

Ferrer I, Nevskaia D, Delasheras C, Sánchez C (1990) About the band gap nature of FeS_2 as determined from optical and photoelectrochemical measurements. Solid State Commun 74:913–916

Jephcoat A, Olson P (1987) Is the inner core of the Earth pure iron? Nature 325:332–335

Karguppikar A, Vedeshwar A (1988) Electrical and optical properties of natural iron pyrite (FeS_2). Phys Status Solidi A Appl Res 109:549–558

Kleppe A, Jephcoat A (2004) High-pressure Raman spectroscopic studies of FeS_2 pyrite. Miner Mag 68:433–441

Lehner S, Savage K, Ayers J (2006) Vapor growth and characterization of pyrite (FeS_2) doped with Co, Ni, and As: variations in semiconducting properties. J Cryst Growth 286:306–317

Lehner S, Newman N, Van S, Bandyopadhyay S, Savage K, Buseck P (2012) Defect energy levels and electronic behavior of Ni-, Co-, and As-doped synthetic pyrite (FeS_2). J Appl Phys 111:083717. doi:10.1063/1.4706558

Li H, Zhang S (2005) Detection of mineralogical changes in pyrite using measurements of temperature-dependence susceptibilities. Chin J Geophys 48:1384–1391

Li M, Gao C, Ma Y, Li Y, Li X, Li H, Liu J, Hao A, He C, Huang X, Zhang D, Yu C (2006) New diamond anvil cell system for in situ resistance measurement under extreme conditions. Rev Sci Instrum 77:123902. doi:10.1063/1.2400669

Merkel S, Jephcoat A, Shu J, Mao H, Gillet P, Hemley R (2002) Equation of state, elasticity, and shear strength of pyrite under high pressure. Phys Chem Miner 29:1–9

Pommier A, Gaillard F, Malki M, Pichavant M (2010) Methodological re-evaluation of the electrical conductivity of silicate melts. Am Miner 95:284–291

Pridmore D, Shuey R (1976) The electrical resistivity of galena, pyrite, and chalcopyrite. Am Miner 61:248–259

Ravindra N, Srivastava V (1981) Temperature-dependence of the energy-gap in pyrite (FeS_2). Phys Status Solidi A Appl Res 65:737–742

Savage K, Stefan D, Lehner S (2008) Impurities and heterogeneity in pyrite: influences on electrical properties and oxidation products. Appl Geochem 23:103–120

Sawaoka A, Inoue K, Saito S (1974) Effect of high pressure on the lattice constants of FeS_2 and CoS_2 having pyrite s tructure. Jpn J Appl Phys 13:579–579

Schieck R, Hartmann A, Fiechter S, Könenkamp R, Wetzel H (1990) Electrical properties of natural and synthetic pyrite (FeS_2) crystals. J Mater Res 5:1567–1572

Sze S, Kwok K (2007) Physics of semiconductor devices, 3rd edn. Wiley, New York, pp 21–22

Utyuzh A (2014) Influence of temperature on Raman spectra of the FeS_2 single crystal with pyrite structure. Phys Solid State 56:2050–2055

Wu L, Dai L, Li H, Zhuang Y, Liu K (2016) Pressure-induced improvement of grain boundary properties in Y-doped $BaZrO_3$. J Phys D Appl Phys 49:345102. doi:10.1088/0022-3727/49/34/345102

Wu L, Dai L, Li H, Hu H, Zhuang Y, Liu K (2017) Anomalous phase transition of Bi-doped Zn_2GeO_4 investigated by electrical conductivity and Raman spectroscopy under high pressure. J Appl Phys 121:125901. doi:10.1063/1.4979311

Yu J, Wu C, Huang Y, Lin S (1992) Electron-paramagnetic-resonance study of the Cr^{3+} and Ni^{2+} ions and the $(SCl)^{2-}$ defect in FeS_2. J Appl Phys 71:370–375